Isolation and Characterization of Functional Oligosaccharides from Soybean Straw: Assessment of Antioxidant and Probiotic Potential

[1-3]Wenming Jiang*, [1]Xingchen Guo, [4]Mingxing Liao, [5]Chunqing Hao, [1]Jingxia Chen, [2]Fang Li**

[1]Chongqing Chemical Industry Vocational College, Chongqing 401228, China.

[2]Chongqing Jiangbei District Disease Prevention Control Center, Chongqing 400020, China.

[3]Chongqing (Changshou) Industrial Technology Research Institute of Green Chemical and New Material, Chongqing 401228, China.

[4]Shaoguan University, Shaoguan 512005, China.

[5]Centre Testing International (Qingdao)Co., Ltd. Qingdao 266108, China.

jwm4617@126.com*

Abstract: Soybean straw was utilized as a raw material to extract hemicellulose by employing an alkaline solution. The structure of polysaccharides was analyzed using UV-visible, infrared, and nuclear magnetic resonance (NMR) one-dimensional and two-dimensional spectra. At the same time, the monosaccharide components and surface structure of xylan in soybean straw were analyzed. The *in vitro* antioxidant activity of soybean straw xylooligosaccharides (XOS) was evaluated using DPPH clearance and reducibility tests. Additionally, the probiotic activity of *Lactobacillus acidophilus* and *Bifidobacterium animalis* was assessed. UV-visible light scanning indicates that the proteins and nucleic acids in the hemicellulose have been removed. High-performance liquid chromatography (HPLC) analysis reveals that soybean straw hemicellulose B primarily consists of L-glucuronic acid, D-mannose, D-mannuronic acid, D-galactose, D-aminogalactose, D-glucose, D-xylose, and L-fucose, with a molar mass ratio of D-xylose at 94.33%. After hydrolysis by xylanase, oligosaccharides with a degree of polymerization of 2-3 are obtained. Scanning electron microscopy (SEM) showed that oligosaccharides were polymerized. Fourier transform infrared (FT-IR) spectroscopy, one-dimensional NMR, and two-dimensional NMR analyses indicate that XOS contain methyl and methoxy groups, and sugar residues are primarily linked through β-1-4 glycosidic bonds. *In vitro* antioxidant tests have shown that soybean straw oligosaccharides exhibit strong DPPH scavenging and reducing abilities. Furthermore, soybean straw oligosaccharides exhibit probiotic activity to *Lactobacillus acidophilus* or *Bifidobacterium animalis*.

Introduction

The production of soybean straw is enormous and has long been overlooked as agricultural waste. However, with the increasingly prominent environmental issues, people have begun to pay attention to the resource utilization of agricultural waste [1]. Soybean straw, as a potential renewable resource, has important components with significant application value. Therefore, conducting in-depth research on the main components of soybean straw and exploring how to achieve its resource utilization have become one of the current research hotspots in the fields of industry and agriculture. Soybean straw is rich in components such as cellulose, hemicellulose, and lignin [2], which can not only be used as raw materials for biofuels and biological fertilizers [3,4]; It

can also be widely applied in fields such as textiles, medicine, and food. Therefore, understanding the main components of soybean straw and exploring its potential utilization value is of great significance for promoting resource recycling and reducing environmental pollution [5]. Among them, hemicellulose is cross-linked with xylan, which can be enzymatically hydrolyzed into XOS [6].

XOS, as a functional polysaccharide and dietary fiber, are widely used as additives [7]. They are characterized by their low calorie content, low viscosity, and stability. Research has shown that oligosaccharides can improve animal growth performance, enhance immunity, and promote the

---

proliferation of bifidobacteria [7-9]. The main sources of preparation are corn cobs, sugarcane bagasse, and straw [10]. Experiments have shown that oligosaccharides have inhibitory effects on *Staphylococcus aureus* [11]; And it can also inhibit inflammation induced by Salmonella [12]. Bifidobacterium exhibits good growth and metabolic characteristics when exposed to XOS [9]. In addition, oligosaccharides have been found to have good antioxidant properties [8], which can regulate blood sugar, lower blood lipids [13,14], and even serve as anti-cancer drugs [15]. In summary, XOS have shown promising application prospects in various biological functions, offering new ideas and possibilities for the advancement of fields such as food, medicine, feed, and cosmetics.

To address the value of sustainable agricultural waste and the increasing demand for prebiotics, XOS were extracted from soybean straw. The primary objectives were to optimize the enzymatic production of XOS, characterize their structural properties, and evaluate their antioxidant and probiotic-stimulating activities to establish their potential for functional food or feed applications. These findings lay the groundwork for transforming soybean straw into high-value bioactive compounds.

Experiment

Extraction of hemicellulose B

After soaking soybean (*Glycine max*) straw powder in a boiling water bath with a 0.3% sodium hydroxide solution for 1 h, the filter residue is obtained through filtration. The residue was extracted by boiling in a water bath with 0.8% ammonium oxalate for 1 h to obtain dietary fiber through filtration. Dietary fiber was further extracted by stirring with a 1.5% sodium hydroxide solution in a 40 °C water bath for 24 h. After filtration, glacial acetic acid was used to adjust the filtrate to a pH of around 5. Subsequently, centrifugation at 5000 rpm for 5 min was carried out to remove the precipitate. The supernatant was added with three times the volume of anhydrous ethanol and refrigerated overnight to precipitate hemicellulose B. After removing the supernatant, the bottom precipitate was centrifuged at 5000 rpm for 5 min [16]. After the polysaccharide precipitate is dissolved in water, the protein in the hemicellulose B solution is removed using the Sevag method. After dialyzing the supernatant (retaining molecules with a molecular weight greater than 3500 D), the hemicellulose B precipitate was obtained through ethanol precipitation

once more. The precipitate dissolves in twice the volume of water and then evaporates to eliminate ethanol. The polysaccharide solution is dissolved completely by adding water, and then freeze-dried.

Protein and nucleic acid testing

Using distilled water as a blank, hemicellulose B is dissolved by distilled water at a concentration ranging from 1 to 2 mg/mL. Subsequently, centrifugation is performed to remove insoluble substances. The supernatant is then scanned using a UV-visible spectrophotometer (UV-1800) within the wavelength range of 200 to 600 nm [17].

Monosaccharide detection

Polysaccharide hydrolysis: 10-20 mg of hemicellulose B was placed in a 10 mL hydrolysis tube, to which 5 mL of 2 mol/L trifluoroacetic acid was added. The tube was sealed with N_2 (10 L/min, 1 min) and hydrolyzed for 2 h in a 110 °C oven. After cooling, 1 mL of hydrolysis solution was taken out and added with 1 mL methanol. The sample is dried with N_2 in a 70 °C water bath. Subsequently, methanol is added again, and the sample is dried with N_2 twice to eliminate trifluoroacetic acid. The tube was added with 1 mL of 0.3 mol/L NaOH solution to dissolve the residue and obtain a polysaccharide hydrolysate. The hydrolysate was then diluted to a certain extent and used for monosaccharide derivatization.

Monosaccharide derivatives: 400 μL of mixed monosaccharide solution or polysaccharide hydrolysate is placed in a stoppered test tube, and then 400 μL of 0.5 mol/L 1-phenyl-3-methyl-5-pyrazolone (PMP) methanol solution is added. The solution was mixed and placed in a 70 °C water bath for 2 h to react. After cooling to room temperature, 400 μL of 0.3 mol/L muriatic acid was added to adjust the pH to 6-7. Subsequently, 1.2 mL of water was added to the solution, followed by an equal volume of chloroform. The mixed liquid is thoroughly blended using a vortex oscillator, and then the chloroform is removed after standing still. The solution was extracted for two times with chloroform as described above. Finally, the solution was filtered using a 0.45 μm aqueous phase membrane for HPLC injection analysis.

Monosaccharide HPLC analysis: Agilent1100 (DAD detector) was used to detect the monosaccharide composition. The chromatographic conditions are presented as follows. A C18 chromatography column (250 mm * 4.6 mm) is

utilized. Mobile phase A consists of a 100 mM sodium phosphate buffer with a pH of 6.7, while mobile phase B is acetonitrile. The detection wavelength is set at 250 nm, and the column temperature is maintained at 30 °C. The flow rate is 1 mL/min, and the injection volume is 5 μL. Regarding the gradient elution conditions, at 0 min, the A/B phase ratio is 86:14 (v/v). At 9 min, this ratio changes to 83:17 (v/v). At 28 minutes, it adjusts to 78:22 (v/v), and at 29 min, it reaches 50:50 (v/v). Finally, at 32 min, the ratio returns to 86:14 (v/v).

Preparation of Xylooligosaccharides

Hemicellulose B (0.5 g) was mixed with 20 mL of pH 4.5 buffer solution. Xylanase was added to the solution to reach 100 U/g of the substrate and hydrolyzed under stirring conditions at 45°C for 1-7 h. After boiling in water for 5 min, the enzymatic solution was centrifuged to remove the precipitate. The reducing sugar content of the supernatant was analyzed by using the 3,5-dinitrosalicylic acid (DNS) method [18]. Sulfuric acid was added to the supernatant to reach a concentration of about 6%, which was hydrolyzed in a boiling water bath for 2 h. The acid hydrolysis solution is neutralized with sodium hydroxide and then filtered. The total sugar content of the filtrate was also determined using the DNS method, and the degree of polymerization was calculated [19]. The appropriate enzymatic hydrolysis time is selected based on the degree of polymerization.

After activation, activated carbon particles are filled into a 22×400 mm chromatography column. According to literature [20], the enzymatic hydrolysate was uniformly loaded onto activated carbon. The chromatography column was first eluted with 300 mL of deionized solution, and then with 400 mL of a 60% ethanol solution. The flow rate of the eluent above is all controlled at 1 mL/min. The ethanol eluent is evaporated to remove ethanol and then freeze-dried for future use.

Characterization of XOS

FT-IR: A XOS sample weighing 0.005 g was mixed with 0.5 g of KBr powder in an agate mortar, ground evenly, and then pressed into a tablet. The FTIR-650 Fourier transform infrared spectrometer was used to scan the transmittance in the wavelength range of 4000-450 cm^{-1}, with KBr as the background [21].

SEM: Five milligrams of dried XOS was attached to a conductive carbon film with double-sided adhesive. Then, the sample was placed in the sample chamber of the ion sputtering equipment. Gold was sprayed onto the sample for approximately 40 seconds. The sample was then observed in the scanning electron microscope observation room (Seiss Sigma 500) with an acceleration voltage of 2 kV [22].

NMR: The 500 MHz nuclear magnetic resonance spectrometer (500 MHz NMR, Bruker) was utilized to record the NMR spectra of soybean straw XOS samples. The sample of 25 mg was dissolved in D$_2$O, and NMR spectra were recorded at 25 °C [23].

In vitro antioxidant activity

DPPH: A 1 mL sample solution was mixed thoroughly with 4 mL of pretreated DPPH ethanol solution (mass fraction 0.004%) in a test tube. Subsequently, the mixture reacted in the dark at room temperature for 30 min. The absorbance of the reaction solution was measured at 517 nm. Each measurement was repeated three times. The calculation of the clearance rate is shown in Formula 1. In the formula, A_0 represents the absorbance value of the DPPH ethanol solution with the same volume of ethanol sample; A_1 represents the absorbance value of the DPPH ethanol solution when the sample is added. A_2 represents the absorbance value of the ethanol solution of the sample when DPPH is not added.

$$E\ (\%) = \frac{A_0 - (A_1 - A_2)}{A_0} \times 100 \qquad \text{Formula 1}$$

Reducibility: 1 mL of the sample solution was mixed with 2.5 mL of 0.2 mol/L phosphate buffer solution (pH 6.6) and 2.5 mL of a 1% mass fraction potassium ferrocyanide solution. The mixture was then incubated at 50 °C for 20 min. After cooling to room temperature, 2.5 mL of a 10% trichloroacetic acid solution, 0.4 mL of a 1% ferric chloride solution, and 4 mL of distilled water were added to the mixture. Afterward, the mixture was allowed to stand and react for 15-20 min. The reaction solution was centrifuged at 3500 rpm for 5 min, and the absorbance of the supernatant was measured at 700 nm. Each group is tested three times, and the calculation formula is shown in Formula 2. In the formula, A_0 is the absorbance value of the solution in the blank group; A_1 is the absorbance value of the sample group; A_2 is the absorbance value of the control group.

$$E(\%) = (1 - \frac{A_1 - A_0}{A_2}) \times 100 \qquad \text{Formula 2}$$

Bacterial activity of XOS

The strain was activated in MRS liquid medium at 37 °C for 48 h, and then reactivated twice in the same way. MRS liquid medium without glucose was prepared and adjusted to pH 6.8. Two 5 mL MRS liquid media were added with 50 mg glucose and XOS respectively, and then sterilized at 121 °C for 15 min. The medium was added with 4% (v/v) activated *Lactobacillus acidophilus* or *Bifidobacterium animalis*. The inoculum was incubated in oscillatory anaerobic culture at 37 °C, and the absorbance of OD600 was measured every 4 h [24].

The strain was activated in MRS liquid medium at 37°C for 48 h, and then reactivated twice using the same method. MRS liquid medium without glucose was prepared and adjusted to pH 6.8. Two 5 mL MRS liquid media were each supplemented with 50 mg glucose and XOS respectively, and then sterilized at 121 °C for 15 min. The medium was supplemented with 4% (v/v) activated *Lactobacillus acidophilus* or *Bifidobacterium animalis*. The inoculum was incubated in oscillatory anaerobic culture at 37 °C, and the absorbance at OD600 was measured every 4 h [24].

Data analysis

All data are presented as mean ± standard deviation. The experiment was conducted three times. ANOVA was employed to analyze the data results. A difference was considered significant when $p < 0.05$.

Results and discussion

Detection of polysaccharide and monosaccharide composition

To determine the removal of proteins and nucleic acids, XOS is typically analyzed using ultraviolet-visible full-wavelength scanning. The maximum absorption wavelengths of nucleic acids and proteins were 260 nm and 280 nm, respectively [25]. Therefore, we can determine whether the proteins and nucleic acids have been completely removed by measuring UV absorption. It can be seen from Fig. 1A that soybean straw XOS does not exhibit any distinct characteristic absorption peaks at 260 nm and 280 nm. This indicates that the protein or nucleic acid in the sample has been removed.
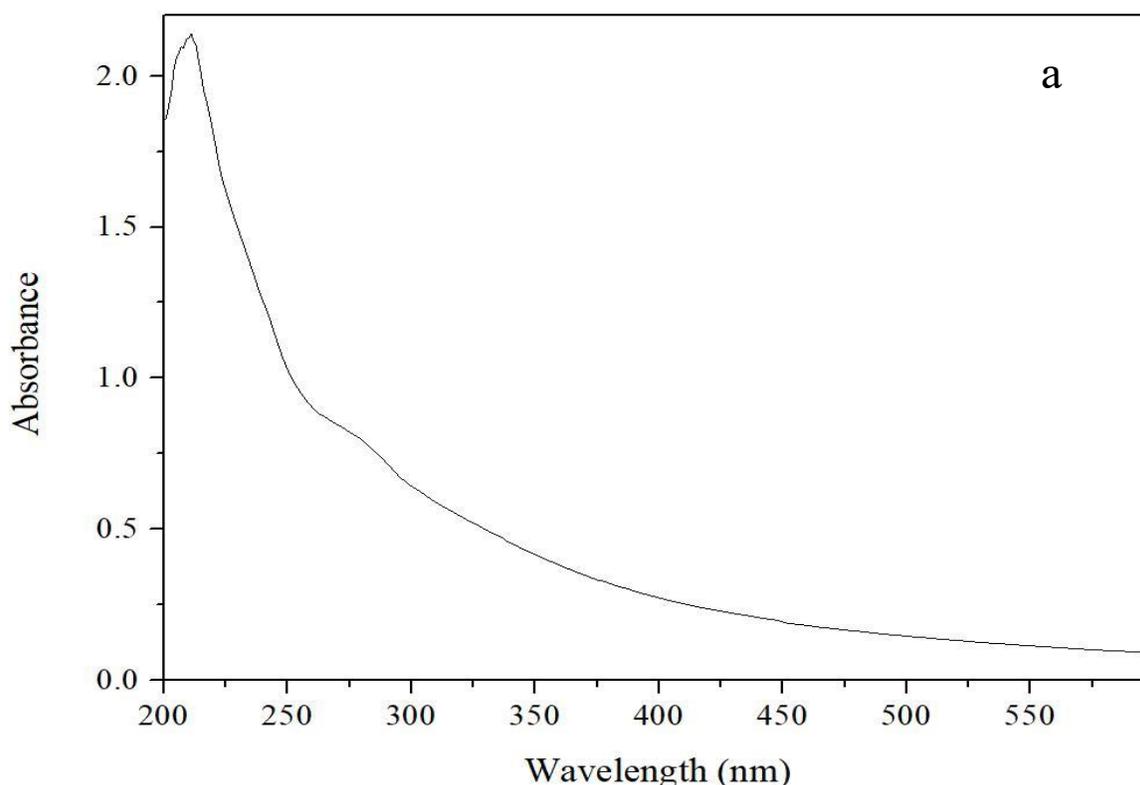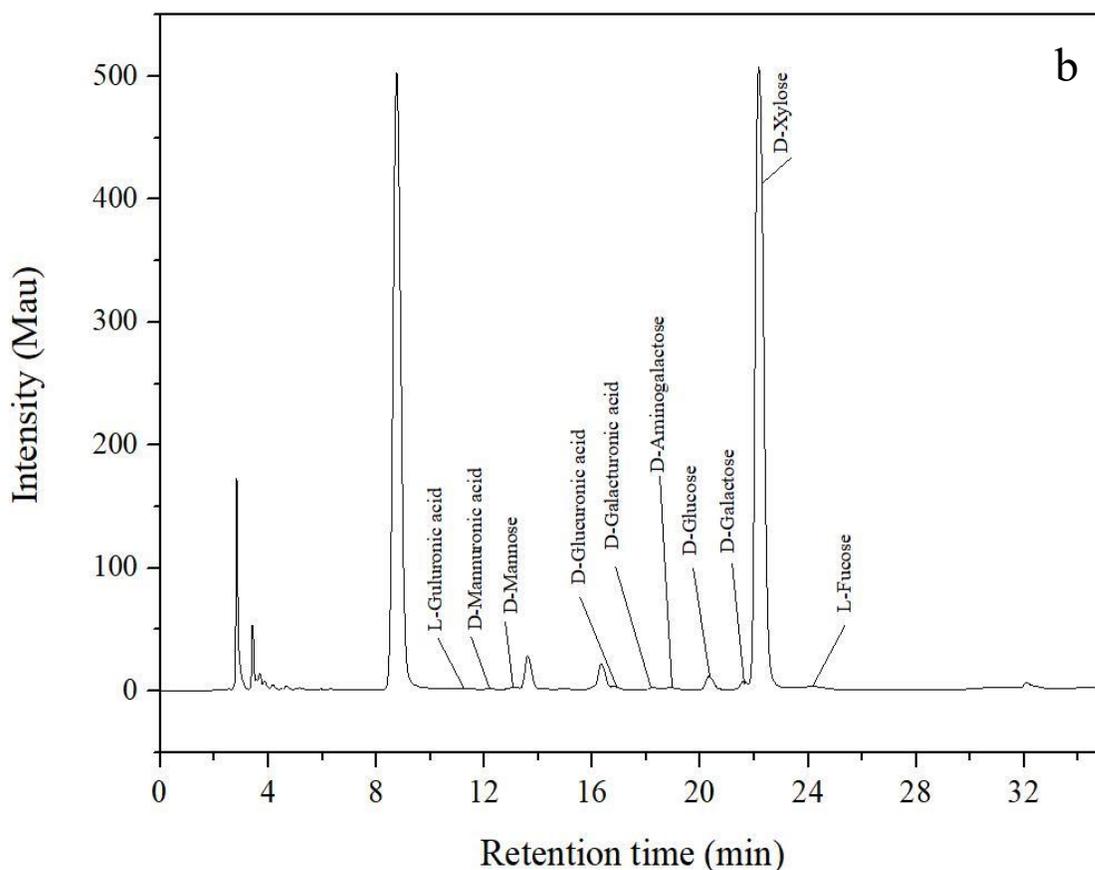
Fig. 1 (a) UV-Vis scanning of hemicellulose B; (b) Monosaccharide analysis of hemicellulose B.

HPLC can be used to analyze the composition of monosaccharides [26]. In this study, hemicellulose B from soybean straw was determined. As shown in Fig. 1B, hemicellulose B is composed of L-guluronic acid, D-mannose, D-mannuronic acid, D-galactose, D-galacturonic acid, D-galactosamine, D-glucose, D-glucuronic acid, D-xylose, and L-fucose, all of which are reductive. Therefore, enzymatic hydrolysis of soybean straw hemicellulose B will release a large amount of reducibility [27]. Xylose content in hemicellulose B was the highest, accounting for 94.332% of the total sugar content, followed by D-glucose. Other monosaccharides and their derivatives are relatively small (Table 1).

Preparation and observation of XOS

The aim of this experiment was to prepare XOS by decomposing hemicellulose B from soybean straw. The prolonged enzymatic hydrolysis will result in an increase in monosaccharide content and a corresponding decrease in XOS content. Insufficient enzymolysis and a high degree of polymerization can result from a too short enzymolysis time. It can be seen from Fig. 2A that the total sugar content started to decrease slowly after 4 h of enzymatic hydrolysis, which may be attributed to the oxidation of some reducing sugars [28]. In the early stage of enzymatic hydrolysis (<4 h), the degree of polymerization decreased significantly. Afterward, the degree of polymerization decreased gradually, possibly attributed to the reduced activity of certain enzymes [29]. The content of reducing sugar increased with the increase in enzymolysis time and remained constant after 6 h. Based on the variations in reducing sugar content and degree of polymerization, the enzymolysis time was determined to be 4-5 h.

In this study, the surface structure of XOS from soybean straw was observed using SEM. Fig. 2B-D shows the surface structure at magnifications of 100, 1000, and 10000 times, respectively. After

magnifying 100 times, the XOS appeared as irregular fragments with a relatively smooth surface. When the magnification is set to 1000, the fracture trace on the surface of XOS can be observed, and the surface is slightly rough. After magnification of 10,000 times, the material surface appears relatively smooth and opaque, possibly as a result of the crosslinking of oligosaccharide molecules during the drying process [30].

Table-1:   Monosaccharide composition of soybean straw hemicellulose B.

Monosaccharide	Retention time	Mass concentration	Mole percent
	min	mg/g	%
L-guluronic acid	11.017	1.062	0.134
D-mannuronic acid	12.123	0.398	0.050
D-mannose	13.108	2.235	0.304
D-glucuronic acid	16.786	2.961	0.374
D-galacturonic acid	18.216	1.371	0.173
D-galactosamine	18.860	2.560	0.291
D-glucose	20.320	20.662	2.813
D-galactose	21.594	4.934	0.672
D-xylose	22.118	577.372	94.332
L-fucose	24.126	5.730	0.856
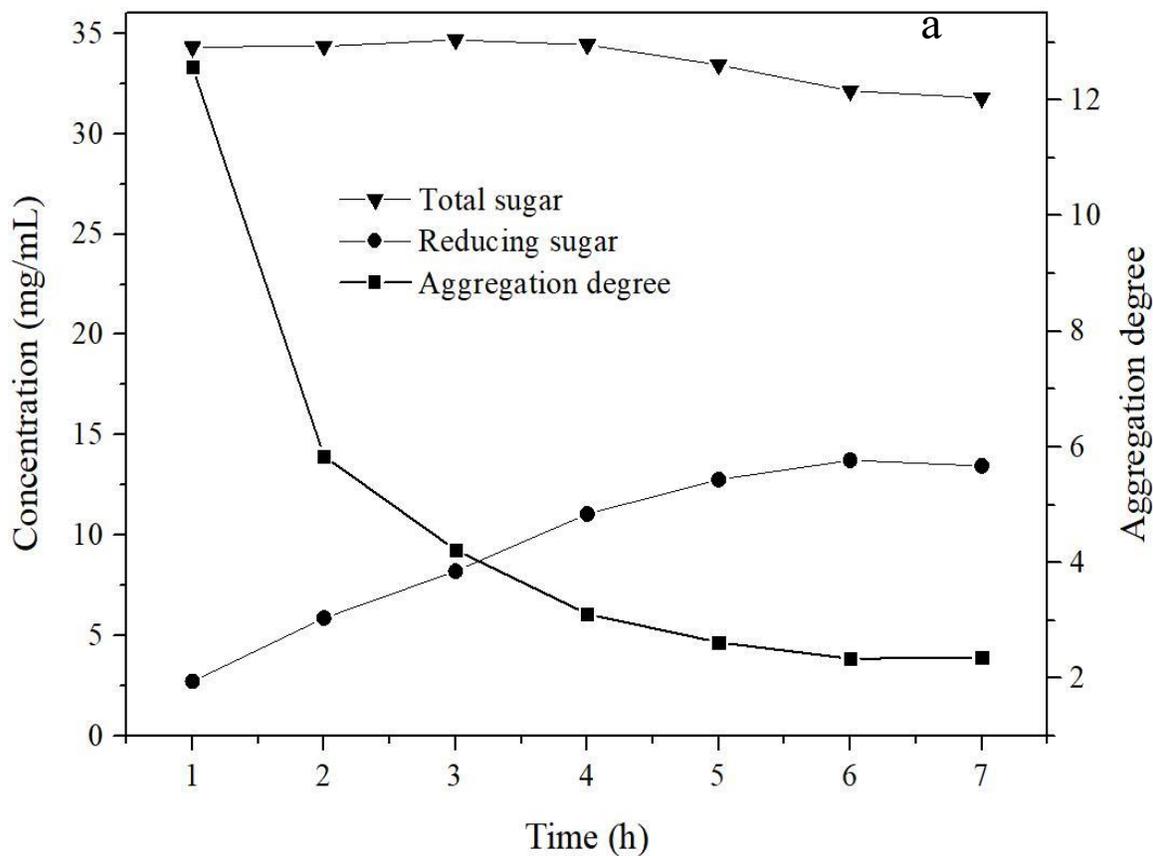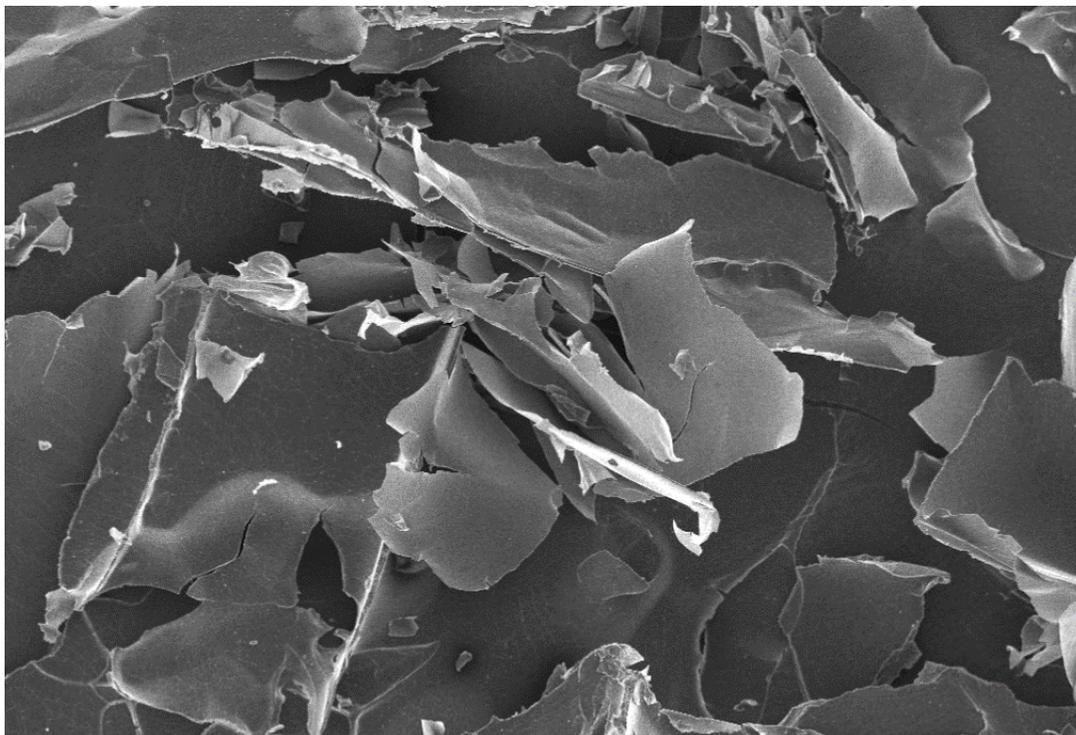
100 µm	EHT = 10.00 kV	Signal A = InLens	Date: 24 Mar 2024	ZEISS
	WD = 6.2 mm	Mag = 100 X	Time: 13:55:01	
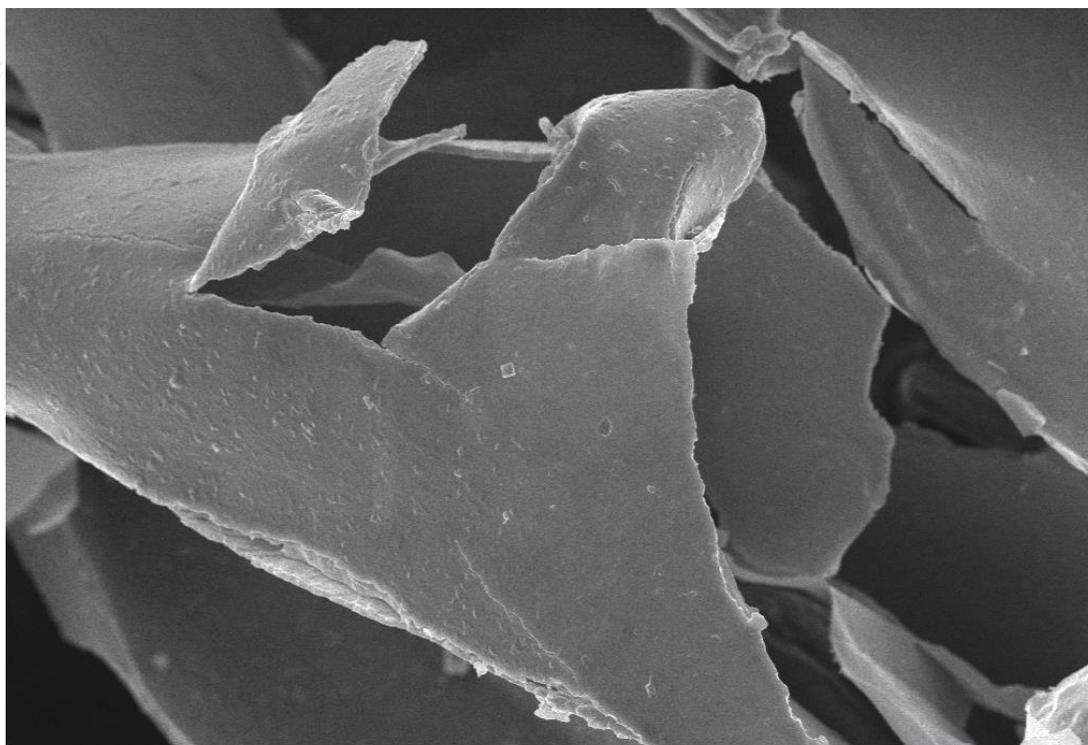
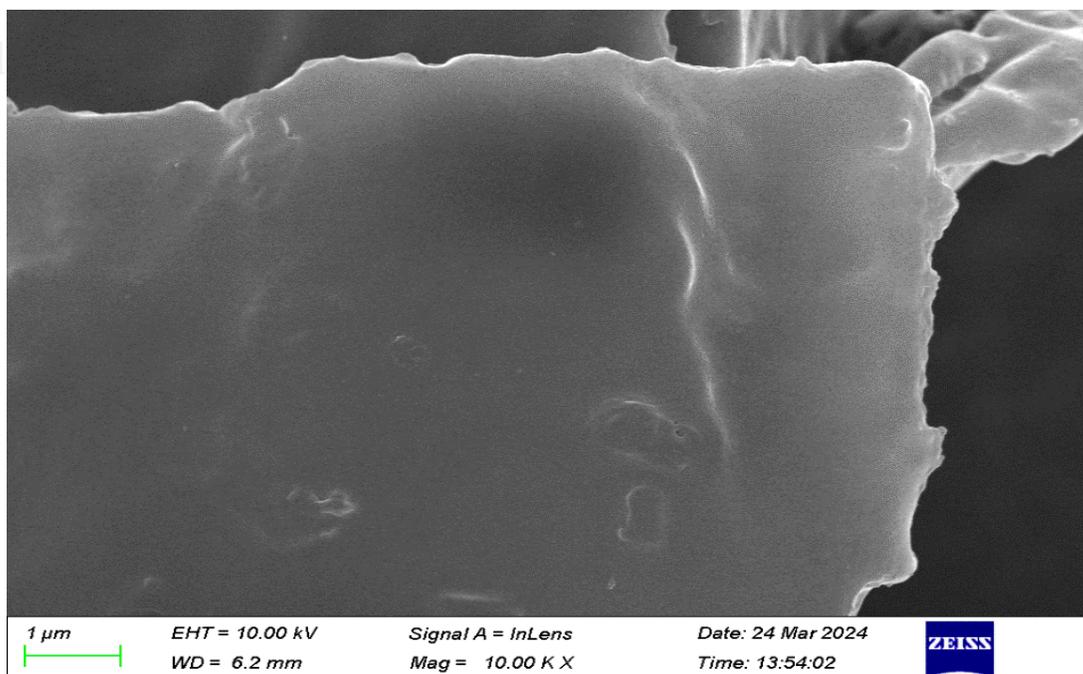| 10 µm	EHT = 10.00 kV	Signal A = InLens	Date: 24 Mar 2024	ZEISS
	WD = 6.2 mm	Mag = 1.00 K X	Time: 13:54:29	

Fig. 2:   (a) Enzymatic hydrolysis of hemicellulose B; SEM images with magnification of 100 (b), 1000 (c) and 10000 (d) times.

FT-IR and one-dimensional NMR analysis

FT-IR is a powerful tool to analyze the structure of matter. It can be seen from Fig. 3 that the absorption peaks of XOS from soybean straw at 3000-3600 cm^{-1} are disordered, including the tensile bending dynamic absorption peak of O-H, the bending vibration absorption peak of -COOH, and the absorption peak of N-H [31,32]. The absorption peak at 2915 cm^{-1} is the tensile vibration absorption peak of C-H [33].The absorption peak at 1633 cm^{-1} corresponds to the stretching vibration absorption peak of -OH [34].The peaks at 1417 cm^{-1} and 1378 cm^{-1} correspond to the bending deformation of -CH$_2$- and the symmetrical deformation of -CH$_3$, respectively [35].The absorption peak at 1245 cm^{-1} corresponds to the C-H bending vibration absorption peak [36].The absorption peaks at 1158 cm^{-1} and 1050 cm^{-1} correspond to C-O absorption on the sugar ring [37,38].The strong characteristic peak at 895 cm^{-1} corresponds to the β-type glycosidic bond [39].

One-dimensional NMR mainly includes ^{1}H NMR, ^{13}C NMR, and DEPT 135, which can be used to assign the chemical shifts of carbon and hydrogen in sugar residues and analyze the types of carbon atoms in oligosaccharides. In this study, the structure of XOS from soybean straw was characterized using one-dimensional NMR. The results are shown in Fig. 3B-D and Table 2.

As can be seen from the ^{1}H NMR spectrum (Fig. 3B), the signals in the ^{1}H NMR are concentrated at 3.16-5.17 ppm, and there are also signal peaks at 1-2 ppm. In general, the chemical shift value of α-type glycosyl isomers is more than 5.0 ppm, while the signal value of β-type glycosyl isomers is less than 5.0 ppm [40].The hydrogen spectrum signals of soybean straw oligosaccharides were mainly concentrated in the range of 4.37-5.17 ppm, indicating that most of the isomers had a β-glycosidic bond configuration and contained a small amount of α-glycosidic bonds.[40] The chemical shift of 3.16 ppm is attributed to the proton on methoxy group. The chemical shift of 3.33-4.02 ppm is mainly attributed to the hydrogen chemical shift on C2-C5 [41]. The hydrogen chemical shift at 4.37-5.17 ppm corresponds to C1. In addition, signal peaks at 1.08–1.20 ppm and 1.95 ppm are present. These are usually characteristic peaks of methyl [42].

The 13C NMR spectra of XOS are shown in Fig. 3C. The chemical shift of C1 is 96.47-100.41 ppm.

The signal peak at 69.16-82.40 ppm corresponds to the chemical shift of C2-C4. The chemical shift of 21.56 ppm was attributed to the methyl group. There is a chemical shift of methylene and methoxy between 58.81 and 65.18. Among them, the chemical shift of 59.86 ppm may belong to methoxy [43].

In DEPT 135, CH and CH3 exhibit positive signal peaks, while CH2 shows negative signal peaks [44]. According to the results of DEPT 135 (as shown in Fig. 3D), the signal at 92.00–101.82 ppm is positive, which is consistent with C1 in the sugar ring. The chemical shift of 69.17-76.37 ppm represents the positive signal peak, corresponding to C2-C4. The chemical shift of 62.96-65.19 ppm represents the negative signal peak, corresponding to pentose C5 [45]. The signal peaks at 60.93 and 59.83 ppm correspond to C6 in certain hexose [46]. The chemical shift of 59.87 ppm was attributed to the methoxy signal peak. The chemical shift of 21.52 ppm corresponds to the signal peak of methyl.

Table-2:   Spectral analysis of XOS.

FT-IR Wavelength (cm^{-1})	Assignment
3000-3600	O-H tensile bending dynamic absorption; -COOH bending vibration absorption; N-H absorption peak
2915	C-H tensile vibration absorption
1633	-OH stretching vibration absorption peak of
1417	-CH$_2$- bending deformation
1378	-CH$_3$ symmetrical deformation
1245	C-H bending vibration absorption
1158, 1050	C-O absorption on the sugar ring
895	β-type glycosidic bond
^{1}H-NMR Chemical shift (ppm)	Assignment
5.09-5.17	Anomeric proton of α-L-arabinofuranose
4.37-4.70	Anomeric proton of β-D-xylopyranose
3.16	Methoxy group
3.33-4.02	Protons on xylose subunits
1.08-1.20，1.95	Characteristic peaks of methyl
* ^{13}C-NMR/DEPT135 Chemical shift (ppm)	Assignment
96.47-100.41	Chemical shift of C1
69.16-82.40	Chemical shift of C2-C4
62.83-65.18	Pentose C5
58.81, 60.91	Hexose C6
59.86	Methoxyl group
21.56	Methyl group

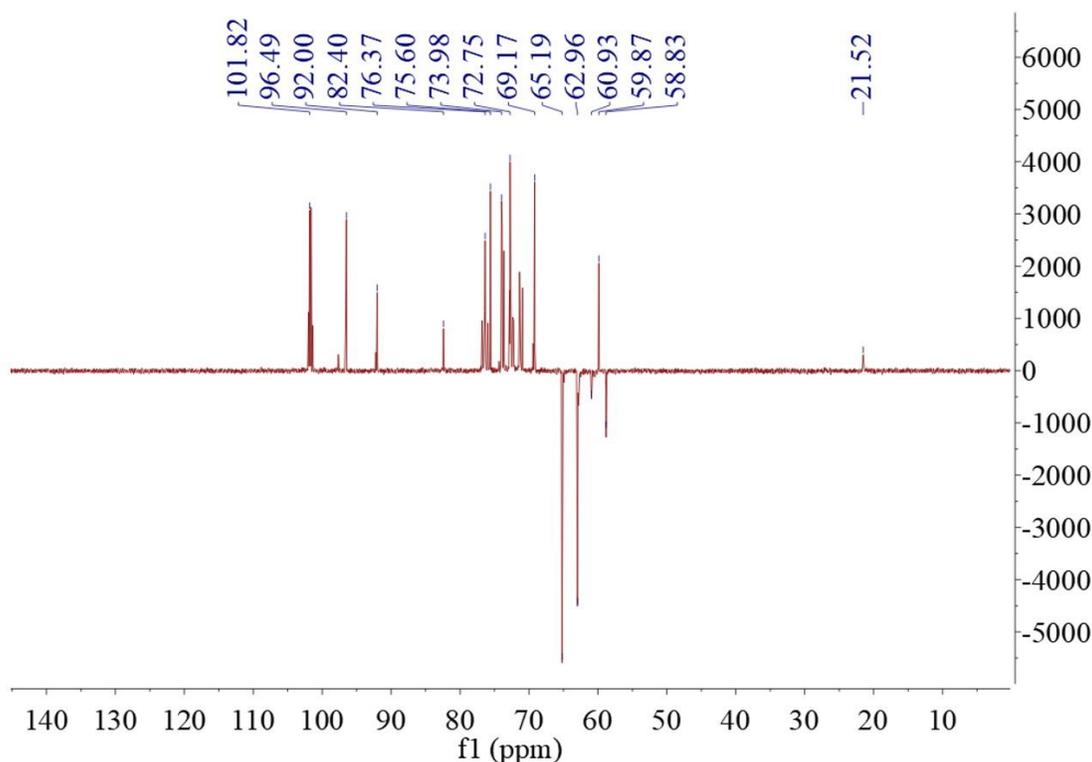* The chemical shift of DEPT135 is analyzed together with ^{13}C NMR

b

c
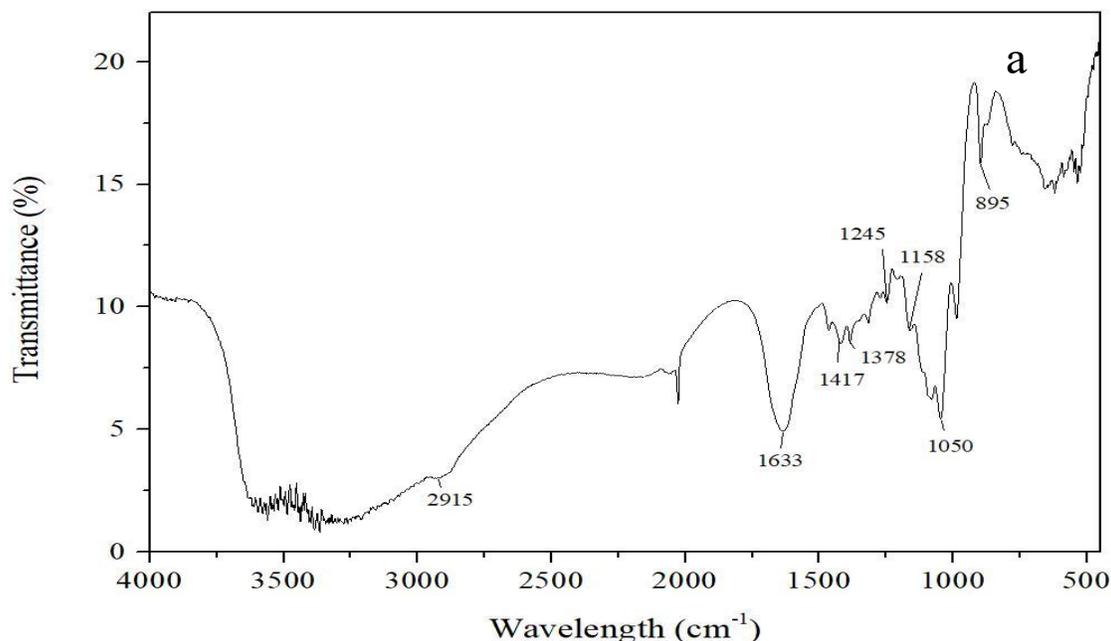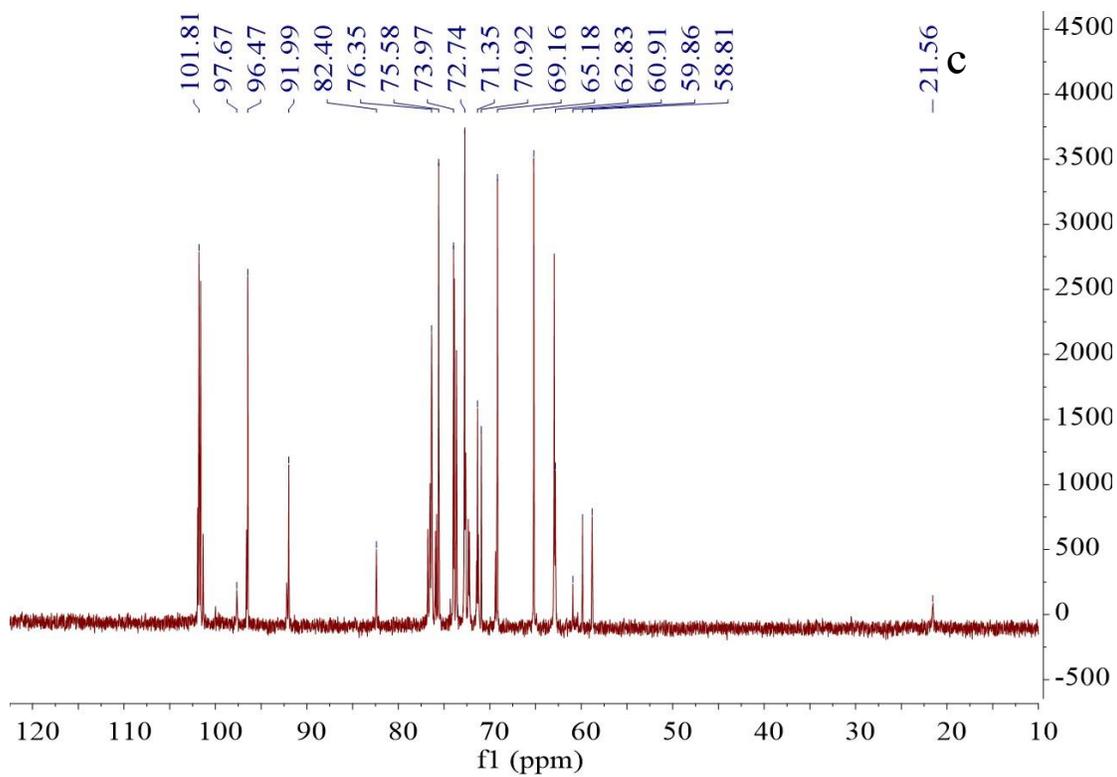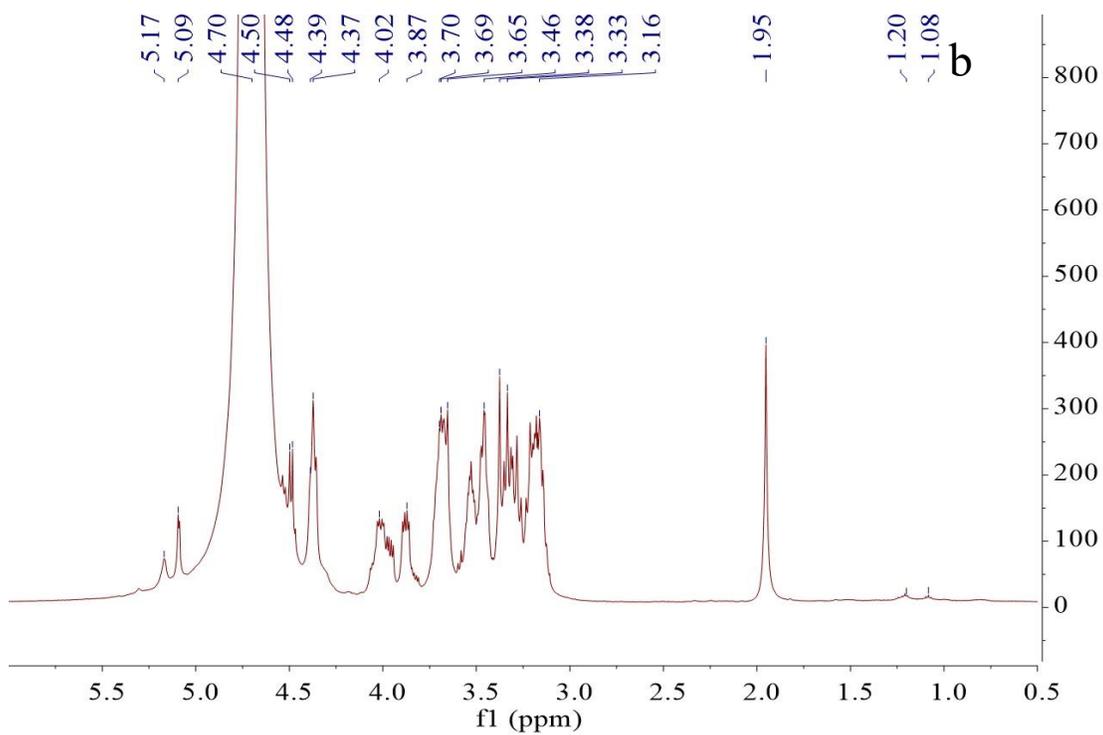
d

Fig. 3:   (a) FT-IR analysis of XOS; [1]H (b), [13]C (c) and dept135 (d) observation of XOS.

Two-dimensiona NMR spectra

Two-dimensional NMR technology plays a crucial role in the analysis of molecular structures. To further analyze the molecular structure of XOS from soybean straw, a two-dimensional NMR analysis was conducted. COSY reflects the coupling relationship between adjacent hydrogen atoms. As can be seen from Fig. 4A, the ^{1}H signal coupling of adjacent carbons is relatively strong. Moreover, it is relatively dense on the diagonal line, which mainly represents the coupling between the hydrogens on xylose C5, methyl, and methoxy [47]. The HSQC spectrum is a correlation spectrum between adjacent C-H atoms [48].

It can be seen from Fig. 4B that XOS contains methyl or methoxy groups. According to the HSQC spectral analysis, the methyl group may connect to the C1 position of the XOS tail sugar residue. The methoxy group may be attached to the C2 position of the tail sugar residue. HMBC spectrum can detect the coupling signal between hydrogen and remote carbon [49]. The linker fragments and sequences of monosaccharide residues can be inferred by coupling heterocephalic hydrogen with carbon linked to another sugar residue. It can be seen from Fig. 4C that sugar residues are connected by 1-4 glycosidic bonds.
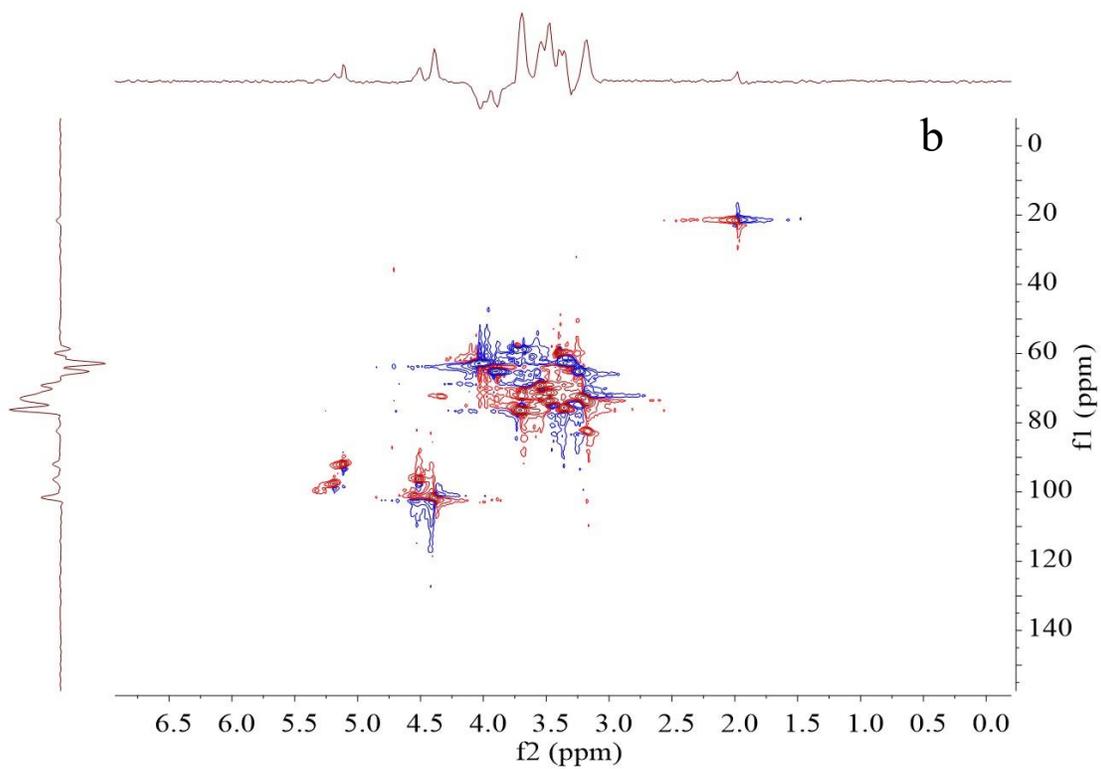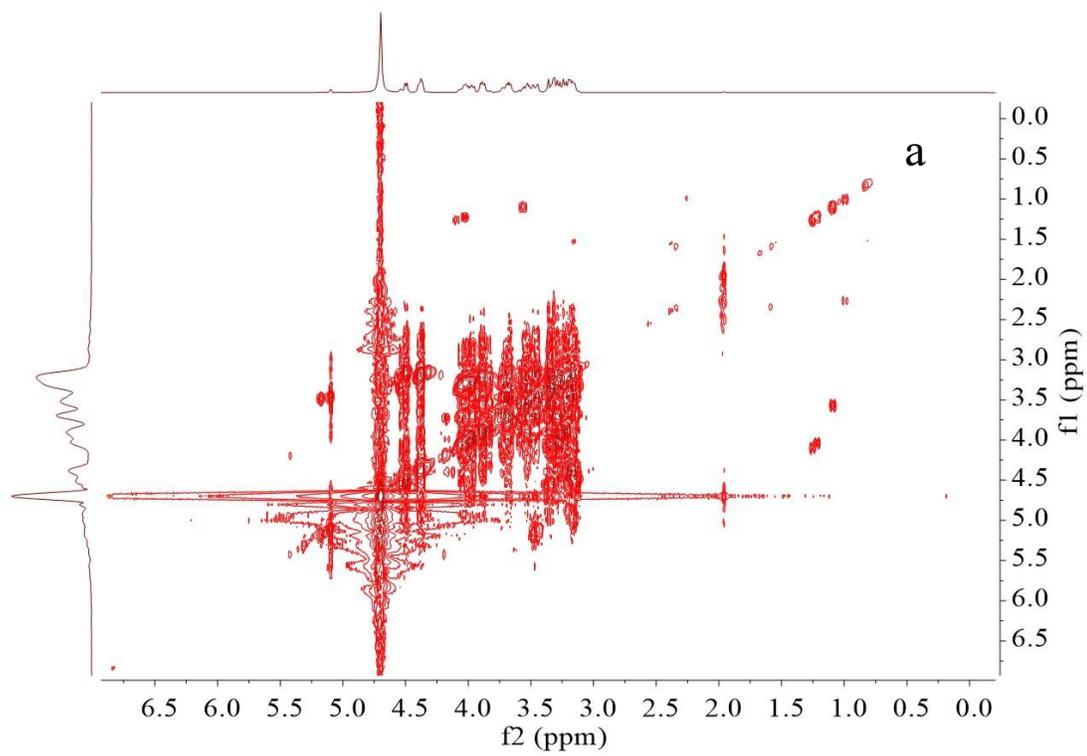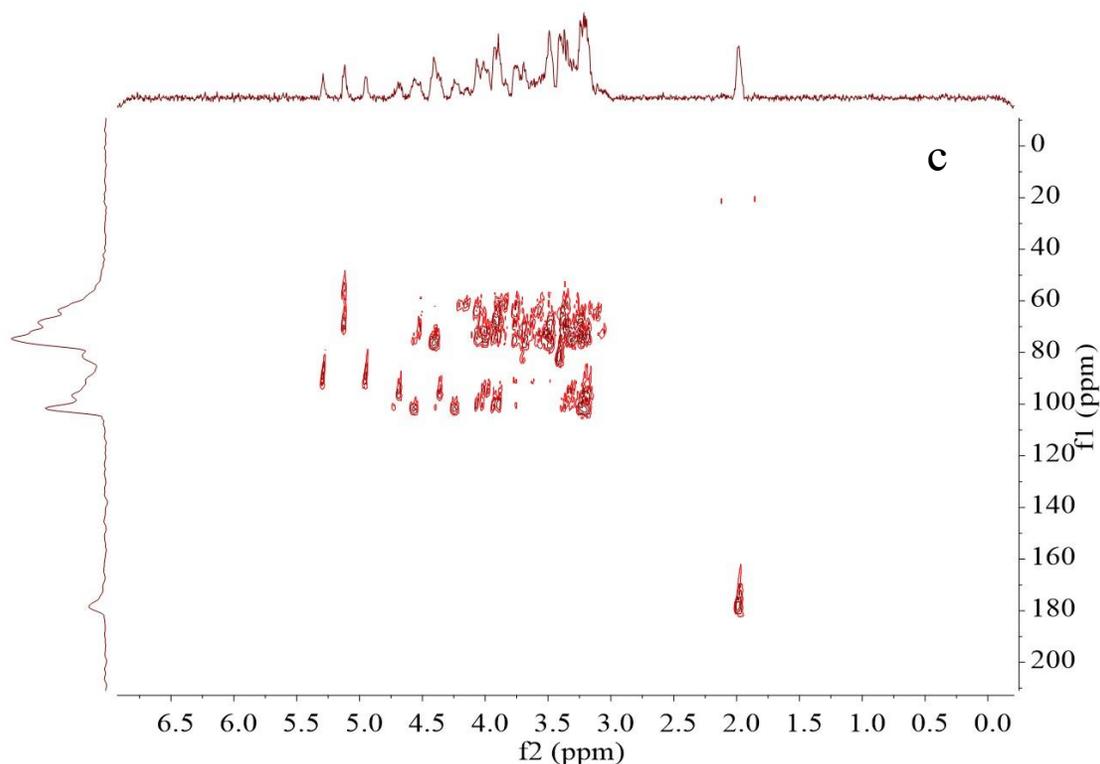
Fig. 4:   COSY (a), HSQC (b), and HMBC (c) analysis of XOS from soybean straw.

Activity verification

Xylan is a type of polysaccharide found in plant cell walls, constituting 15% to 35% of the plant cell's dry weight, and serving as the primary component of plant hemicellulose B. XOS generated through its breakdown exhibit strong antioxidant and probiotic properties. In this study, the antioxidant activity was evaluated through DPPH clearance and reduction ability, while the beneficial activity was assessed using *Lactobacillus acidophilus* and *Bifidobacterium animalis* (Fig. 5). It can be seen from the figure that as the concentration increases, the antioxidant activity and reducibility of soybean straw hemicellulose B and XOS also increase. When the concentration reached 3.2 mg/mL, the activity did not increase. Comparatively, XOS has higher activity than hemicellulose B, which indicates that the enzymatic hydrolysis reaction releases the reducing hemiacetal hydroxyl [50]. Taking *Lactobacillus acidophilus* as the research subject, the study examined the growth-promoting effect of XOS derived from soybean straw. It can be seen from Fig. 5C that XOS and glucose exhibited a clear ability to enhance production during the initial stage of strain growth. In the early stage of fermentation, glucose has a better growth-promoting effect. During the later stage of fermentation, XOS and glucose exhibited similar growth-promoting effects. According to the results of a study on the impact of soybean straw XOS on the growth of *Bifidobacterium animalis in vitro*, it was found that XOS and glucose exhibited a similar growth-promoting effect during the initial stage of fermentation. XOS showed a higher growth-promoting effect in the late fermentation stage. Therefore, XOS has a probiotic-promoting effect on *Lactobacillus acidophilus* and *Bifidobacterium animalis* [51].
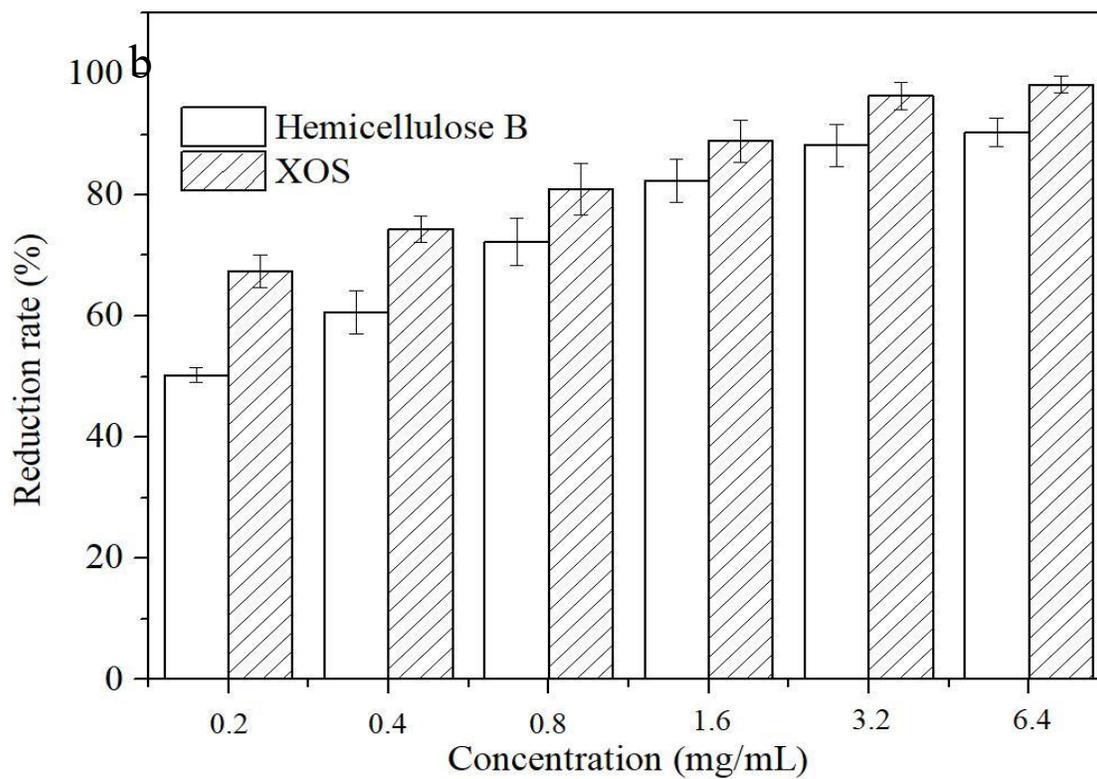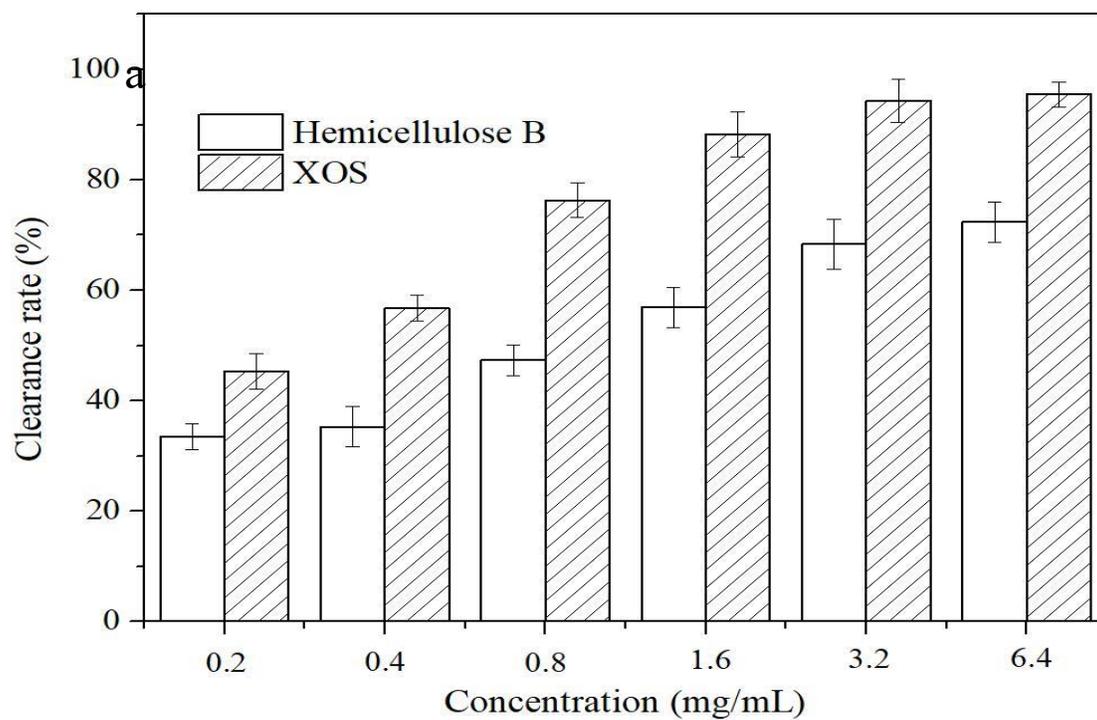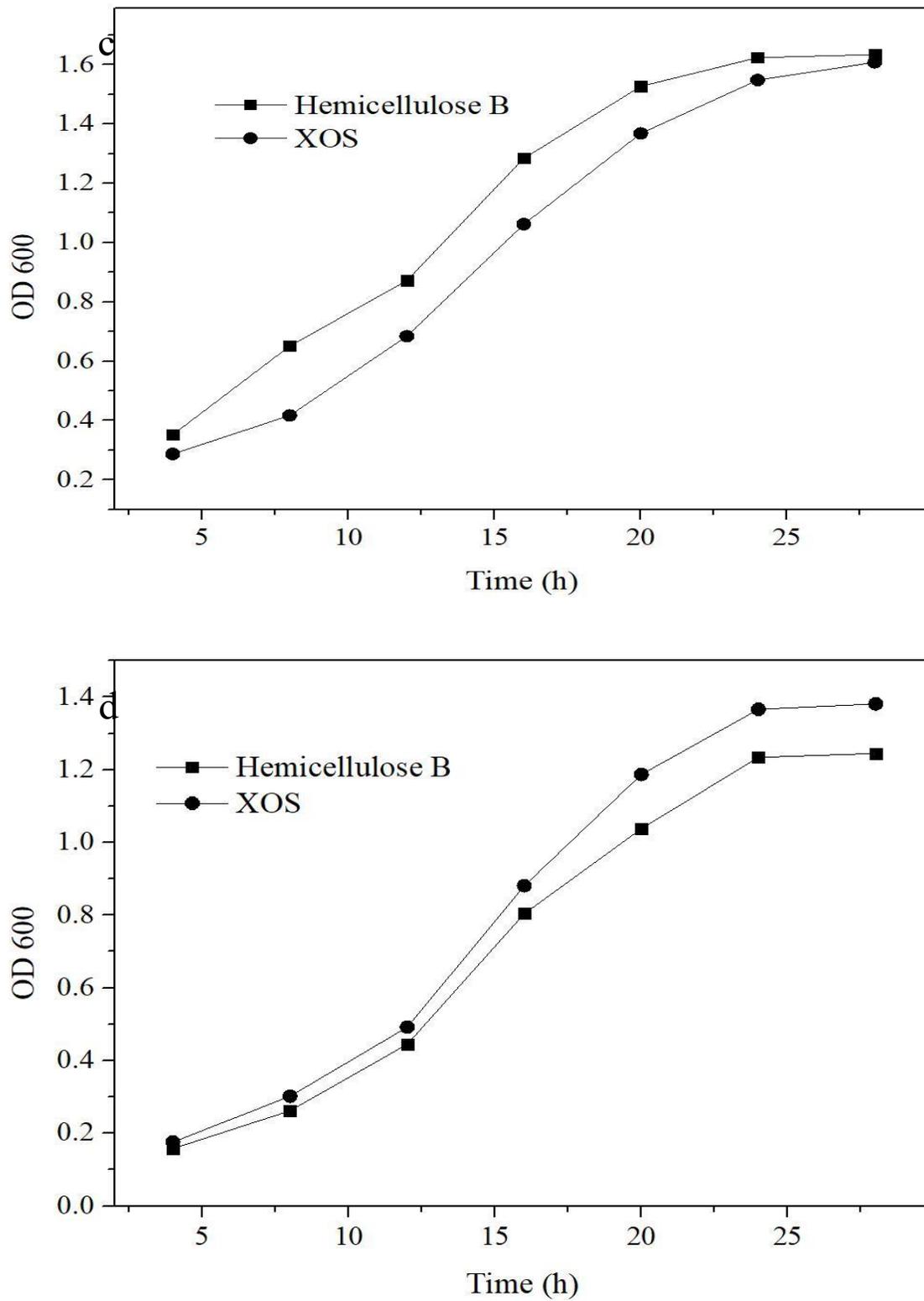
Fig. 5: DPPH clearance (a) and reducibility (b) of XOS; Probiotic activity of XOS to *Lactobacillus acidophilus* (c) and *Bifidobacterium animalis,*

Conclusion

To enhance the economic value of soybean straw, XOS was prepared from soybean straw. Soybean straw hemicellulose B was extracted using an alkali solution. After UV-Vis full-wavelength scanning, no significant absorption peaks were found at 260 and 280 nm, indicating that proteins and nucleic acids had been removed by the Sevage method. After the hydrolysis of soybean straw hemicellulose B, HPLC analysis revealed that soybean straw hemicellulose B mainly consisted of L-guluronic acid, D-mannose, D-mannuronic acid, D-galactose, D-galacturonic acid, D-galactosamine, D-glucose, D-glucuronic acid, D-xylose, and L-fucose. The molar mass ratio of D-xylose is 94.33%. XOS with a degree of polymerization of 2-3 were obtained through xylanase hydrolysis. SEM analysis revealed that XOS had polymerized, resulting in an opaque and smooth surface. FT-IR, one-dimensional NMR, and two-dimensional NMR analyses revealed that XOS contained methyl and methoxy groups, and sugar residues were primarily connected by β-1-4 glycosidic bonds. Antioxidant tests conducted *in vitro* demonstrated that soybean straw XOS exhibited strong DPPH scavenging ability and reducibility. In addition, XOS also has probiotic activities of *Lactobacillus acidophilus* and *Bifidobacterium animalis*. In conclusion, this study provides an experimental basis for the utilization of XOS from soybean straw.

Acknowledgements

References

1. J. Zhang, Q. Zhang, J. Wang, X. Shi, and Z. Zhang, Analysis of the monosaccharide composition of fucoidan by precolumn derivation HPLC, *Chin. J. Oceanol. Limn.,* **27**: 578 (2009).

2. C. De Pretto, R. D. L. C. Giordano, P. W. Tardioli, & C. B. B. Costa, Possibilities for producing energy, fuels, and chemicals from soybean: a biorefinery concept. *Waste Biomass Valori.,* **9**: 1703 (2018).

3. F. Vedovatto, C. Bonatto, S. F. Bazoti, B. Venturin, S. L. Alves Jr, A. Kunz, R. L. Steinmetz, H. Treichel, M. A. Mazutti, G. L. Zabot, & M. V. Tres, Production of biofuels from soybean straw and hull hydrolysates obtained by subcritical water hydrolysis. *Bioresource Technol.,* **328**: 124837 (2021).

4. Y. Fu, H. Gao, H. Yu, Q. Yang, H. Peng, P. Liu, Y. Li, Z. Hu, R. Zhang, J. Li, & Z. Qi, Specific lignin and cellulose depolymerization of sugarcane bagasse for maximum bioethanol production under optimal chemical fertilizer pretreatment with hemicellulose retention and liquid recycling. *Renew. Energ.,* **200**: 1371 (2022).

5. Z. F. Xue, W. C. Cheng, L. Wang, & G. Song, Improvement of the shearing behaviour of loess using recycled straw fiber reinforcement. *KSCE J. Civ. Eng.,* **25**: 3319 (2021).

6. P. Kundu, S. K. Kansal, & S. Elumalai, Synergistic action of alkalis improve the quality hemicellulose extraction from sugarcane bagasse for the production of xylooligosaccharides. *Waste Biomass valori.,* **12**: 3147 (2021).

7. D. Luo, J. Li, T. Xing, L. Zhang, & F. Gao, Combined effects of xylo-oligosaccharides and coated sodium butyrate on growth performance, immune function, and intestinal physical barrier function of broilers. *Anim. Sci. J.,* **92**: e13545 (2021).

8. X. Liu, R. Cao, & Y. Xu, Acidic hydrolyzed xylo-oligosaccharides bioactivity on the antioxidant and immune activities of macrophage. *Food Res. Int.,* **163**: 112152 (2023).

9. W. Yi, Q. Wang, Y. Xue, H. Cao, R. Zhuang, D. Li, J. Yan, J. Yang, Y. Xia, & F. Zhang, Xylo-oligosaccharides improve functional constipation by targeted enrichment of Bifidobacterium. *Food Sci. & Nutr.,* **12**: 1119 (2024).

10. L. Dyshlyuk, E. Ulrikh, S. Agafonova, & O. Kazimirchenko, Xylooligosaccharides from Biomass Lignocellulose: Properties, Sources and Production Methods. *Reviews in Agricultural Science,* **12**: 1 (2024).

11. Z. Sun, Z. Yue, E. Liu, X. Li, & C. Li, Assessment of the bifidogenic and antibacterial activities of xylooligosaccharide. *Front. Nutr.,* **9**: p.858949 (2022).

12. J. Pang, S. Wang, Z. Wang, Y. Wu, X. Zhang, Y. Pi, D. Han, S. Zhang, & J. Wang, Xylo-oligosaccharide alleviates Salmonella induced inflammation by stimulating Bifidobacterium animalis and inhibiting Salmonella colonization. *The FASEB Journal,* **35**: e21977 (2021).

13. W. H. H. Sheu, I. T. Lee, W. Chen, & Y. C. Chan, Effects of xylooligosaccharides in type 2 diabetes mellitus. *J. Nutr. Sci. Vitaminol.,* **54**: 396 (2008).

14. J. Wang, Y. Cao, C. Wang, & B. Sun, Wheat bran xylooligosaccharides improve blood lipid

metabolism and antioxidant status in rats fed a high-fat diet. *Carbohyd. Polym.,* **86**: 1192 (2011).

15. P. K. Gupta, P. Agrawal, P. Hedge, & M. S. Akhtar, Xylooligosaccharides and their anticancer potential: an update. *Anticancer Plants: Natural Products and Biotechnological Implements,* **2**: 255 (2018).

16. W. Jiang, M.S. Thesis, *Xylanase preparation by Aspergillus niger ATCC16404 fermentation of soybean hull and production of xylo-oligosaccharide*, Jinan University, (2011).

17. H. Li, X. Wang, Q. Xiong, Y. Yu, & L. Peng, Sulfated modification, characterization, and potential bioactivities of polysaccharide from the fruiting bodies of Russula virescens. *Int. J. Biol. Macromol.,* **154**: 1438 (2020).

18. R. Hu, L. Lin, T. Liu, P. Ouyang, B. He, & S. Liu, Reducing sugar content in hemicellulose hydrolysate by DNS method: a revisit. *J. Biobased Mater. Bio.,* **2**: 156 (2008).

19. A. Fuso, F. Rosso, G. Rosso, D. Risso, I. Manera, & A. Caligiani, Production of xylo-oligosaccharides (XOS) of tailored degree of polymerization from acetylated xylans through modelling of enzymatic hydrolysis. *Food Res. Int.,* **162**: 112019 (2022).

20. C. Nobre, J. A. Teixeira, & L. R. Rodrigues, Fructo-oligosaccharides purification from a fermentative broth using an activated charcoal column. *New biotechnol.,* **29**: 395 (2012).

21. P. E. Imoisili, K. O. Ukoba, & T. C. Jen, Synthesis and characterization of amorphous mesoporous silica from palm kernel shell ash. *boletín de la sociedad española de cerámica y vidrio*, **59**: 159 (2020).

22. D. Talmi-Frank, Z. Altboum, I. Solomonov, Y. Udi, D. A. Jaitin, M. Klepfish, E. David, A. Zhuravlev, H. Keren-Shaul, D. R. Winter, & I. Gat-Viks, Extracellular matrix proteolysis by MT1-MMP contributes to influenza-related tissue damage and mortality. *Cell host microbe,* **20**: 458 (2016).

23. X. Ji, J. Guo, D. Ding, G. Jie, L. Hao, X. Guo, & Y. Liu, Structural characterization and antioxidant activity of a novel high-molecular-weight polysaccharide from Ziziphus Jujuba cv. Muzao. *J. Food Meas. Charac.,* **16**: 2191 (2022).

24. S. Li, R. Huang, N. P. Shah, X. Tao, Y. Xiong, & H. Wei, Antioxidant and antibacterial activities of exopolysaccharides from Bifidobacterium bifidum WBIN03 and Lactobacillus plantarum R315. *J. Dairy Sci.,* **97**: 7334 (2014).

25. P. Arvind, S. Priyadarshini, B. Duraiswamy, S. P. Dhanabal, & G. Ramu, UV Detection and Avoidance of Protein in Basella alba leaf Mucilage Polysaccharide by differential precipitation. *Research Journal of Pharmacy and Technology,* **14**: 3093 (2021).

26. J. B. Zhang, C. Dai, Z. Wang, X. You, Y. Duan, X. Lai, R. Fu, Y. Zhang, M. Maimaitijiang, K. H. Leong, & Y. Tu, Resource utilization of rice straw to prepare biochar as peroxymonosulfate activator for naphthalene removal: Performances, mechanisms, environmental impact and applicability in groundwater. *Water Res.,* **244**: 120555 (2023).

27. C. Valls, F. J. Pastor, T. Vidal, M. B. Roncero, P. Díaz, J. Martínez, & S. V. Valenzuela, Antioxidant activity of xylooligosaccharides produced from glucuronoxylan by Xyn10A and Xyn30D xylanases and eucalyptus autohydrolysates. *Carbohyd. Polym.,* **194**: 43 (2018).

28. R. Saini, R. R. Singhania, A. K. Patel, C. W. Chen, & C. D. Dong, A circular biorefinery approach for the production of xylooligosaccharides by using mild acid hydrothermal pretreatment of pineapple leaves waste. *Bioresource Technol.,* **388**: 129767 (2023).

29. J. R. Büttler, T. Bechtold & T. Pham, Efficient and simple method for the quantification of alkyl polyglycosides by hydrolysis and photometric determination of reducing sugars. *Arab. J. Chem.,* **15**: 104102 (2022).

30. P. Penksza, R. Juhász, B. Szabó-Nótin, & L. Sipos, Xylo-oligosaccharides as texture modifier compounds in aqueous media and in combination with food thickeners. *Food Sci. Nutr.*, **8**: 3023 (2020).

31. F. Nejatzadeh-Barandozi, & S. T. Enferadi, FT-IR study of the polysaccharides isolated from the skin juice, gel juice, and flower of Aloe vera tissues affected by fertilizer treatment. *Org. med. Chem. Lett.,* **2**: 1 (2012).

32. L. Carson, C. Kelly-Brown, M. Stewart, A. Oki, G. Regisford, Z. Luo, & V. I. Bakhmutov, Synthesis and characterization of chitosan-carbon nanotube composites. *Mater. Lett.,* **63**: 617 (2009).

33. I. A. Nehdi, H. Sbihi, C. P. Tan, H. Zarrouk, M. I. Khalil, & S. I. Al-Resayes, Characteristics, composition and thermal stability of Acacia senegal (L.) Willd. seed oil. *Ind. Crop. Prod.,* **36**: 54 (2012).

34. N. Thombare, A. Mahto, D. Singh, A. R. Chowdhury, & M. F. Ansari, Comparative FTIR characterization of various natural gums: a criterion for their identification. *J. Polym. Environ.,* **31**: 3372 (2023).

35. Q. Zeng, Y. Wang, A. Javeed, F. Chen, J. Li, Y.

Guan, B. Chen, & B. Han, Preparation and properties of polyvinyl alcohol/chitosan-based hydrogel with dual pH/NH_3 sensor for naked-eye monitoring of seafood freshness. *Int. J. Biol. Macromol.,* p.130440 (2024).

36. A. D. Rajora, & T. Bal, Evaluation of cashew gum-polyvinyl alcohol (CG-PVA) electrospun nanofiber mat for scarless wound healing in a murine model. *Int. J. Biol. Macromol.,* **240**: p.124417 (2023).

37. M. Szymańska-Chargot, P. Pękala, A. Siemińska-Kuczer, & A. Zdunek, A determination of the composition and structure of the polysaccharides fractions isolated from apple cell wall based on FT-IR and FT-Raman spectra supported by PCA analysis. *Food Hydrocolloid.,* **150**: p.109688 (2024).

38. M. Chylińska, M. Szymańska-Chargot, & A. Zdunek, FT-IR and FT-Raman characterization of non-cellulosic polysaccharides fractions isolated from plant cell wall. *Carbohyd. Polym.,* **154**: 48 (2016).

39. T. Hong, J. Y. Yin, S. P. Nie, & M. Y. Xie, Applications of infrared spectroscopy in polysaccharide structural analysis: Progress, challenge and perspective. *Food chem. X,* **12**: p.100168 (2021).

40. S. Q. Huang, J. W. Li, Y. Q. Li, & Z. Wang, Purification and structural characterization of a new water-soluble neutral polysaccharide GLP-F1-1 from Ganoderma lucidum. *Int. J. Biol. Macromol.,* **48**: 165 (2011).

41. P. Kaur & R. Kaur, Valorization of rice straw via production of modified xylans and xylooligosaccharides for their potential application in food industry. *Cellulose Chemistry Technology*, **56**: 293 (2022).

42. H. N. Cheng, & T. G. Neiss, Solution NMR spectroscopy of food polysaccharides. *Polym. Rev.* **52**: 81 (2012).

43. T. Fischer, A. Yair, M. Veste, & H. Geppert, Hydraulic properties of biological soil crusts on sand dunes studied by 13C-CP/MAS-NMR: A comparison between an arid and a temperate site. *Catena,* **110**: 155 (2013).

44. L. M. Cordeiro, V. de Fátima Reinhardt, C. H. Baggio, M. F. de Paula Werner, L. M. Burci, G. L. Sassaki & M. Iacomini, Arabinan and arabinan-rich pectic polysaccharides from quinoa (Chenopodium quinoa) seeds: Structure and gastroprotective activity. *Food Chem.,* **130**: 937 (2012).

45. P. Kovač, J. Hirsch, A. S. Shashkov, A. I. Usov, & S. V. Yarotsky, ^{13}C-NMR spectra of xylo-oligosaccharides and their application to the elucidation of xylan structures. *Carbohydrate Research*, **85**: 177 (1980).

46. Y. Xie, Y. Liu, C. Jiang, H. Wu, & S. Bi, The existence of cellulose and lignin chemical connections in ginkgo traced by 2H-13C dual isotopes. *Bioresources*, **15**: 9028 (2020).

47. I. Speciale, A. Notaro, P. Garcia-Vello, F. Di Lorenzo, S. Armiento, A. Molinaro, R. Marchetti, A. Silipo, & C. De Castro, Liquid-state NMR spectroscopy for complex carbohydrate structural analysis: A hitchhiker's guide. *Carbohyd. Polym*., **277**: 118885(2022).

48. E. G. Shakhmatov, P. V. Toukach, S. P. Kuznetsov, & E. N. Makarova, Structural characteristics of water-soluble polysaccharides from Heracleum sosnowskyi Manden. *Carbohyd. Polym*., **102**: 521 (2014).

49. P. Talamond, L. Mondolot, A. Gargadennec, A. D. Kochko, S. Hamon, A. Fruchier, & C. Campa, First report on mangiferin (C-glucosyl-xanthone) isolated from leaves of a wild coffee plant, Coffea pseudozanguebariae (Rubiaceae). *Acta Bot. Gallica.,* **155**: 513 (2008).

50. N. Yu, H. Peng, L. Qiu, R. Wang, C. Jiang, T. Cai, Y. Sun, Y. Li, & H. Xiong, New pectin-induced green fabrication of Ag@ AgCl/ZnO nanocomposites for visible-light triggered antibacterial activity. *Int. J. Biol. Macromol.,* **141**: 207 (2019).

51. H. Mäkeläinen, M. Saarinen, J. Stowell, N. Rautonen, & A. C. Ouwehand, Xylo-oligosaccharides and lactitol promote the growth of Bifidobacterium lactis and Lactobacillus species in pure cultures. *Benef. Microbes,* **1**: 139 (2010).